R. & M. No. 3294

MINISTRY OF AVIATION

AERONAUTICAL RESEARCH COUNCIL
REPORTS AND MEMORANDA

Measurement of the Pitching-Moment Derivatives for Rigid Tapered Wings of Hexagonal Planform Oscillating in Supersonic Flow

By L. Woodgate, J. F. M. Maybrey and C. Scruton, B.Sc.
of the Aerodynamics Division, N.P.L.

LONDON: HER MAJESTY'S STATIONERY OFFICE
1962
THIRTEEN SHILLINGS NET

Measurement of the Pitching-Moment Derivatives for Rigid Tapered Wings of Hexagonal Planform Oscillating in Supersonic Flow

By L. Woodgate, J. F. M. Maybrey and C. Scruton, B.Sc.
of the Aerodynamics Division, N.P.L.

*Reports and Memoranda No. 3294**
March, 1961

Summary. Pitching-moment derivatives have been measured, using a free-oscillation technique, for a series of thin tapered wings with both streamwise and raked tips. Wings of three aspect ratios ($A.R.$ = 2·74, 2·00 and 1·25) were tested with three positions of the pitching axis (h = 0·4, 0·5 and 0·6). The Mach number ranged from 1·38 to 2·47 and the Reynolds number and frequency parameter were less than 1·6 × 10^6 and 0·03 respectively. Tunnel boundary-layer effects were avoided by the use of reflection plates. A smaller test programme was also carried out on the effects of a body (non-oscillating) in close proximity to the wing with two alternative nose shapes.

The theory predicted the trends of the derivative variation with Mach number. The numerical agreement was much improved when allowances were made in the theory for finite thickness of the wings. The effect of the body on the derivatives was very small; the only significant difference found was in the stiffness derivative at h = 0·4.

1. *Introduction.* A previous report[1] describes measurements of pitching-moment derivatives on rectangular wings oscillating in supersonic flow. The present report describes a similar programme of tests on a series of tapered wings differing in aspect ratio and planform. The investigation was initiated to provide data on the oscillatory derivatives of the control surfaces of missiles, and the basic planform of the models with raked tips was chosen to be representative of a class of control fins used on missiles. Later, the family of wing planform tested was adopted as a subject for a systematic study of the various methods of calculating the derivatives. In the report the experimental values are compared with those calculated by Lehrian[2]. The influence of a body (non-oscillating) with two alternative nose shapes was also investigated. The tests were carried out in the N.P.L. 11 in. Supersonic Wind Tunnel. The measurements were made by the free-oscillation method using half-span models mounted on reflection plates to by-pass the tunnel boundary layer.

The tapered wings (*see* Fig. 2) had a double-wedge section with a constant thickness/chord ratio of 0·05. The basic planform was successively cropped to provide planforms of seven different shapes and three different spans. All the planforms were oscillated about the mid-chord axis; in addition planforms with streamwise tips oscillated about the h = 0·4 and h = 0·6 axes and those with raked tips were oscillated about either the h = 0·4 axis or the h = 0·6 axis according to the direction of raking.

* Previously issued as A.R.C. 22,683. Published with the permission of the Director, National Physical Laboratory.

The Reynolds number of the tests ranged from $1{\cdot}53 \times 10^6$ to $1{\cdot}01 \times 10^6$ and the frequency parameter was about $0{\cdot}03$.

2. *Basic Formulae.* The aerodynamic moment acting on the wing is written

$$\mathscr{M} = M_\theta\theta + M_{\dot\theta}\dot\theta$$

and for simple harmonic motion of frequency $\omega/2\pi$, $\mathscr{M}$ is expressed in terms of its non-dimensional in-phase and out-of-phase components as

$$\mathscr{M} = \rho V^2 c_r S(m_\theta + i\nu m_{\dot\theta})\theta$$

where $\nu = \omega c_r/V$.

The equation of motion of the wing performing free oscillations in pitching moment against a spring constraint is then

$$I\ddot\theta + (K - M_{\dot\theta})\dot\theta + (\sigma - M_\theta)\theta = 0.$$

On substitution of the solution

$$\theta = \theta_0 e^{\mu t}\sin\omega t$$

and assuming, as was found in the experiments, that $\mu^2 - \mu_0^2 \ll \omega^2 - \omega_0^2$ and $\mu_0^2 \ll \omega_0^2$ the following expression for M_θ and $M_{\dot\theta}$ are found

$$-M_\theta = \frac{\sigma}{f_0^2}(f - f_0)(f + f_0)$$

$$-M_{\dot\theta} = 2I[f\delta - f_0\delta_0]$$

where the suffix 0 denotes quantities measured *in vacuo*.

3. *Description of Apparatus.* 3.1. *The Wind Tunnel.* The tests were carried out in the N.P.L. continuous-flow wind tunnel which had a 12 in. by 11 in. working section for the range of $1{\cdot}35 < M < 1{\cdot}7$ and a 14 in. by 11 in. section for the range $1{\cdot}7 < M < 2{\cdot}5$. The tunnel stagnation pressure could be reduced from one to about one quarter of an atmosphere. Tunnel humidity was controlled by introducing dry air both before and during the run, the surplus air being extracted by pumps. Following the experience gained in previous tests on the effects of humidity, the tests were carried out only when the frost point was $-15°$F or less.

3.2. *The Reflection Plates.* It was necessary to have separate reflection plates for each of the two tunnel Mach number ranges mentioned above. This was not only because of the difference in the working-section dimensions but also because of considerations concerning the interference of the flow over the wing by disturbances from the leading edges of the plate after reflection from the tunnel walls. Due to these limitations, it was not possible to make the plate for the lower Mach number range large enough to accommodate a body and even for the higher Mach number range the length of the body was necessarily smaller than was desired. Details of the two plates are given in Fig. 1.

3.3. *Model Wings and Body.* The details of the basic wing planform and of the successive changes made by cropping the wing are given in Fig. 2. With streamwise tips, the tapered wings had a symmetrical double-wedge section of constant thickness/chord ratio of $0{\cdot}05$ for their entire

length. The wings with raked tips were formed simply by cutting off the tip at the appropriate angle. Thus for wings with streamwise and with raked tips the tip edge was of finite thickness. Most tests were carried out with these blunt side edges. One planform ($A.R. = 2{\cdot}0$, $\psi = 30°$) was also tested with the tip chamfered to a sharp edge. The chamfering was such that the 5% symmetrical double-wedge chordwise section was then maintained over the whole wing (Fig. 3). To enable tests to be made about pitching axes of $h = 0{\cdot}4$, $0{\cdot}5$ and $0{\cdot}6$, two wing models of identical planform and section were made, one had the attachment flange in the centre of the chord and on the second model the flange was off-set so that it could be pitched about either $h = 0{\cdot}4$ or $h = 0{\cdot}6$ axis by simply rotating the model through 180° about its pitching axis. (Fig. 3.)

To distinguish between tests with the wing adjacent to the body and the wing alone, the latter are referred to as 'plain wings'. The diameter of the half-cylindrical body which was fixed directly to the layer reflection plate was $2\frac{1}{2}$ in. Two alternative nose shapes could be fitted to this body, one was a 15° cone and the other an ogival shape (Fig. 1). Details of the wing planforms tested in conjunction with a body are given in Fig. 4. With one exception these tests were restricted to planforms with streamwise tips and to pitching axes of $h = 0{\cdot}4$ and $h = 0{\cdot}5$. Changes of the pitching axis were made by a shift in the position of the wing, the axis remaining in a fixed location relative to the tunnel, and to the rear part of the body which was common for all the axis positions. To maintain the same flow conditions over the wing when the pitching axis was changed, a nose piece with a parallel portion of different length was fitted so that the nose of the body remained in the same position relative to the wing.

3.4. *Model Mounting.* The mounting was the same as used in the previous tests[1]. The arrangement is shown diagrammatically in Fig. 5 and a photograph of the mounting is reproduced in Fig. 6. The oscillating system was mounted on a rigid bracket fixed to the tunnel wall and consisted essentially of a cylinder suspended on two cross-spring bearings and a torque bar to provide the required stiffness against rotation of the cylinder. A continuous hole through the tunnel wall, through the reflection plate and its support and through the body when used, allowed the wing to be attached to the oscillating cylinder by means of a 1 in. diameter steel rod. The gap between the rod and the hole was $\frac{1}{32}$ in. but air leakage through this gap was prevented by enclosing the mounting in an airtight box. The system was made to oscillate by means of a spring-loaded plunger which operated against an arm attached to the rotating cylinder.

3.5. *Measuring and Recording Equipment.* The electronic equipment was very similar to that used in the previous tests[1]. The motion of the wing was recorded by means of a simple condenser gauge, the moving vanes of which were attached to the cylinder and the fixed vanes to the framework of the surrounding airtight box. This gauge was used in conjunction with the Southern Instruments frequency-modulation equipment to produce a d.c. voltage proportional to the angular displacement of the wing. This signal was displayed on a cathode-ray oscilloscope and a film record of the decaying oscillations was made by photographing the screen with a continuously moving film camera. In the previous tests[1] the frequency of the oscillation was measured by displaying $0{\cdot}01$ sec time pulses on the second beam of the oscilloscope. This facility was retained for the present tests but it was found more accurate and convenient to measure the frequency by means of a photo-electric pick-up and an electronic frequency meter which counted the number of $0{\cdot}001$ sec pulses, derived from the N.P.L. Standard-frequency supply, occurring in a pre-set number of model oscillations.

4. *Method of Test.* Film records of the decaying oscillations of the wing in supersonic flow of Mach numbers 1·38 to 2·47 were obtained, and these were analysed in a specially designed optical viewer on which the peak-to-peak amplitude of individual cycles could be measured. These amplitudes were then plotted against cycle number on logarithmic graph paper and the logarithmic decrements for various amplitudes were determined from the slope of the graph. The frequencies of the oscillations were measured on the electronic frequency meter. By means of a cylindrical container which could be placed over but not touching the wing and which sealed itself against the reflection plate, it was possible to evacuate the whole of the space surrounding the oscillating system to an absolute pressure of just under 1 in. of mercury. The values of the apparatus damping and the *in vacuo* moment of inertia were then determined by free-oscillation tests. A similar cylindrical container with semi-circular cut-outs on the sides, permitted the same tests to be made for the wing-body combinations. However, due to the sealing difficulties between the body and the container it was only possible to achieve a pressure of 1·75 in. of mercury.

5. *Results.* As in the previous tests[1] the values of the damping derivative $-m_{\dot{\theta}}$ were found to be dependent on the amplitude θ whereas there was very little variation with amplitude in the value of the stiffness derivative $-m_{\theta}$. For some of the tests the value of $-m_{\dot{\theta}}$ remained constant for a considerable part of the amplitude range; for others the value was found to vary approximately linearly with amplitude. For all tests the result quoted is the mean value for the whole amplitude range ($0{\cdot}006 < \theta < 0{\cdot}03$ approximately). It was noted that for those tests in which the value of $-m_{\dot{\theta}}$ remained constant for a range of amplitude, the mean value differed little from the constant value.

The values of $-m_{\theta}$ and $-m_{\dot{\theta}}$ for plain wings are given in Tables 1 to 5 inclusive and those for wing-body combinations in Tables 6, 7 and 8. The results for plain wings are plotted against Mach number in Figs. 7 to 20 inclusive, together with the values calculated for a 'flat plate' wing by linearised theory[2] and also with these values modified by a theoretical allowance for the effect of the finite thickness of the wing. Interpolated results for $M = 1{\cdot}4$ and $M = 2{\cdot}4$ for planforms with streamwise tips are plotted against aspect ratio in Figs. 21 and 22 and for planforms with raked tips interpolated results for $M = 1{\cdot}4$ are plotted against ψ, the angle of tip cut-off, in Figs. 23 and 24. The results for wings with streamwise tips in combination with the body and the 15° conical nose are plotted against Mach number in Figs. 23 and 24, together with the corresponding experimental and theoretical values for the plain wing. The effect of nose shape is shown in Figs. 27 and 28 where the results for wings with streamwise tips in combination with the body are given, the body being fitted with either the 15° conical nose or the ogival nose. A similar comparison made for a wing with raked tip is given in Fig. 29.

6. *Discussion of Results.* 6.1. *Plain Wings.* In comparison with the values calculated for 'flat plate' wings by linearised theory[2] the experimental values of the stiffness derivative $-m_{\theta}$, were always more negative by an average of 0·055 at $M = 1{\cdot}4$ and 0·040 at $M = 2{\cdot}4$. When the thickness corrections were applied, these average differences were reduced to 0·025 at $M = 1{\cdot}4$ and 0·020 at $M = 2{\cdot}4$. In the few cases where the flat-plate theory gave values in very close agreement with the experimental values, the comparison with the thickness-corrected theory was not so good.

The agreement between experimental and calculated values was usually better for the damping than for the stiffness derivative. The measured values of the damping derivative were more positive

than those calculated by flat-plate theory, the difference being about $0{\cdot}035$ at $M = 1{\cdot}4$ and $0{\cdot}004$ at $M = 2{\cdot}4$. Incorporation of the thickness corrections to the calculated values was again beneficial and reduced the average differences to $0{\cdot}020$ at $M = 1{\cdot}4$ and $0{\cdot}003$ at $M = 2{\cdot}4$. The small discrepancies which remain between the experimental and theoretical values might be attributed to some of the following factors.

(*a*) *Model flexibility.* The *A.R.* $2{\cdot}74$ wing was not stiff enough to prevent flexing due to the aerodynamic forces. This was made evident by small displacements of the pitching axis observed at the tip. However, the small-aspect ratio-wings were much stiffer and with the *A.R.* $1{\cdot}25$ wing there was no evidence of any flexing. It was not considered worth-while attempting to apply corrections for the effect of model flexibility. Accurate corrections would have been difficult to calculate and from the results for the *A.R.* $2{\cdot}74$ and *A.R.* $1{\cdot}25$ wings (Figs. 7, 8, 11 and 12) it would appear that the discrepancies between theory and experiment were not significantly worse for the higher-aspect-ratio wing. The large discrepancy at $M = 1{\cdot}4$ and $h = 0{\cdot}6$ found for the *A.R.* $2{\cdot}74$ wing is similar to that found previously on the two-dimensional double-wedge aerofoil[3] and was attributed to effects of bow-wave detachment and viscosity.

(*b*) *Viscosity effects.* The theory is based on potential-flow considerations and makes no allowance for viscosity effects which may cause boundary layers and flow separations. The boundary layer permits pressure fluctuations from behind the trailing-edge shocks to travel upstream and thus modify the pressure distributions. The variation of $-m_{\dot{\theta}}$ with amplitude is also attributed to these effects.

(*c*) *Tip effect.* The theory does not allow for any change in the direction of the flow over the tip. As the aspect ratio decreases the effect of the tip would be expected to become progressively more important. However, there is no significant difference in the agreement between the theoretical and the experimental values for either the low- or high-aspect-ratio wings (Figs. 7, 8, 11 and 12). It would be expected that wings with raked tips would show more influence of the tip than those with streamwise tips. This was not found to be so for the stiffness derivative (Fig. 23). The damping derivative shows a small variation with ψ, but this is not consistent for all aspect ratios (Fig. 24).

(*d*) *Blunt side edges.* The theory is not valid for wings with the blunt edges leading; the experimental results for this case are therefore compared with the theoretical values for wings with sharp leading side edges. The theory could be used for wings with blunt trailing edges but the difference in the theoretical values for blunt and sharp trailing edges proved to be negligible for all planforms tested. In the experimental tests in which results for wings with blunt and sharp side edges were compared (Figs. 17 and 18), very little difference in the values of the derivatives was found when the side edge was leading (Fig. 17). With the side edges trailing the wing with blunt edges gave better agreement with theory than that with a sharp edge (Fig. 18).

6.2. *Wing-body combinations.* In Figs. 25 and 26 the stiffness and damping derivatives for wings adjacent to a cylindrical body are compared with the corresponding plain-wing measured values and also the values calculated by thickness-corrected theory for plain wings. The body made no measurable difference with axis at $h = 0{\cdot}5$ but with $h = 0{\cdot}4$ the values of the stiffness derivative are consistently more negative than those for the plain wing. Change of nose shape from the 15° cone to an ogival shape (Figs. 27, 28 and 29) produced no significant changes in the measured derivative values. For the one planform with a raked tip tested (*A.R.* $= 2{\cdot}74$ and $\psi = 30°$, *see* Fig. 29) it

was found that there was no significant difference in the value of stiffness derivative from the corresponding case with a streamwise tip, but there was a small difference in the value of the damping derivative at the lowest Mach number. A similar difference in $-m_{\dot{\theta}}$ was found with the plain wings.

7. *Conclusions.*

(*a*) The flat-plate linearised theory predicted the trends of the variation of derivatives with Mach number but the numerical values, especially for the stiffness derivatives, were not in close agreement.

(*b*) In most cases the application of thickness corrections to the calculated values resulted in much better agreement with the experimental values. The experimental and calculated values for the damping derivatives were in very good agreement.

(*c*) The effect on the derivatives of a cylindrical body in close proximity to the wing was very small.

NOTATION

M		Mach number
V		Wind speed
ρ		Air density
c		Wing chord
c_r		Root chord (for wing-body combinations, the chord adjacent to the body surface)
S		Total area of half wing excluding projection into body
s		Wing semi-span. For the present purpose this is taken to be the distance between the inboard and outboard edges of the half-wing model used, and does not include the body radius
$A.R.$	$=$	$2s/c_r$, aspect ratio
ψ		Angle of tip cut-off, denoted positive when tip edge is leading and negative when trailing
h		Distance between the axis of rotation and the leading edge of the wing at the root divided by the root chord
I		Moment of inertia of the oscillating system
σ		Elastic-stiffness coefficient of the oscillating system
K		Apparatus damping coefficient
$-M_\theta$		Aerodynamic-stiffness derivative
$-m_\theta$	$=$	$-M_\theta/\rho V^2 c_r S$, non-dimensional form of $-M_\theta$
$-M_{\dot\theta}$		Aerodynamic-damping derivative
$-m_{\dot\theta}$	$=$	$-M_{\dot\theta}/\rho V c_r^2 S$, non-dimensional form of $-M_{\dot\theta}$
f		Frequency of oscillation
ω	$=$	$2\pi f$, angular frequency
ν	$=$	$\omega c_r/V$, frequency parameter
δ		Logarithmic decrement of the oscillations (natural logarithm of the ratio of the amplitude of successive cycles of oscillation)
θ		Angular displacement in pitching motion (radians)
		Suffix 0 applied to quantities f, ω, δ, denotes the values assumed by these quantities for tests *in vacuo*

REFERENCES

No.	*Author*	*Title, etc.*
1	C. Scruton, L. Woodgate, K. C. Lapworth and J. F. M. Maybrey	Measurements of the pitching moment derivatives for rigid wings of rectangular planform oscillating about the mid-chord axis in supersonic flow. A.R.C. C.P. 594. March, 1961.
2	Doris E. Lehrian	Calculation of stability derivatives for tapered wings of hexagonal planform oscillating in a supersonic stream. A.R.C. R. & M. 3298. September, 1960.
3	C. Scruton, L. Woodgate, K. C. Lapworth and J. F. M. Maybrey	Measurement of pitching-moment derivatives for aerofoils oscillating in two-dimensional supersonic flow. A.R.C. R. & M. 3234. January, 1959.

TABLE 1

Measured Values of the Derivatives $-m_\theta$ and $-m_{\dot\theta}$ for Plain Tapered Wings of Symmetrical 5% Double-Wedge Section with Blunt Streamwise Tips

A.R. = 2·74

M	$h = 0{\cdot}4$		$h = 0{\cdot}5$		$h = 0{\cdot}6$	
	$-m_\theta$	$-m_{\dot\theta}$	$-m_\theta$	$-m_{\dot\theta}$	$-m_\theta$	$-m_{\dot\theta}$
1·38	0·099	−0·024	−0·108	0·068	−0·292	0·254
1·58	0·092	+0·017	−0·070	0·047	−0·210	0·127
1·75	0·068	+0·021	−0·061	0·043	−0·182	0·093
1·97	0·061	+0·039	−0·054	0·047	−0·152	0·085
2·16	0·049	+0·033	−0·054	0·043	−0·139	0·064
2·44	0·037	+0·031	−0·037	0·038	−0·132	0·059

A.R. = 2·00

M	$h = 0{\cdot}4$		$h = 0{\cdot}5$		$h = 0{\cdot}6$	
	$-m_\theta$	$-m_{\dot\theta}$	$-m_\theta$	$-m_{\dot\theta}$	$-m_\theta$	$-m_{\dot\theta}$
1·38	0·047	0·023	−0·119	0·095	−0·286	0·160
1·58	0·080	0·050	−0·067	0·047	−0·202	0·111
1·75	0·043	0·047	−0·060	0·055	−0·176	0·111
1·97	0·044	0·040	−0·059	0·056	−0·159	0·082
2·16	0·035	0·042	−0·055	0·045	−0·127	0·083
2·47	0·030	0·044	−0·045	0·045	−0·126	0·082

A.R. = 1·25

M	$h = 0{\cdot}4$		$h = 0{\cdot}5$		$h = 0{\cdot}6$	
	$-m_\theta$	$-m_{\dot\theta}$	$-m_\theta$	$-m_{\dot\theta}$	$-m_\theta$	$-m_{\dot\theta}$
1·38	−0·047	0·160	−0·158	0·215	−0·277	0·275
1·58	+0·012	0·103	−0·106	0·107	−0·216	0·160
1·75	−0·001	0·073	−0·095	0·076	−0·185	0·109
1·97	+0·011	0·069	−0·084	0·066	−0·165	0·095
2·16	+0·006	0·058	—	—	−0·147	0·087
2·47	+0·014	0·051	−0·064	0·063	−0·134	0·065

TABLE 2

Measured Values of the Derivatives $-m_\theta$ and $-m_{\dot\theta}$ for Plain Tapered Wings of Symmetrical 5% Double-Wedge Section with Leading Side Edges ($\psi = +30°$)

(*a*) blunt side edges

A.R. = 2·74, $\psi = +30°$

M	$h = 0·5$		$h = 0·6$	
	$-m_\theta$	$-m_{\dot\theta}$	$-m_\theta$	$-m_{\dot\theta}$
1·38	−0·101	0·050	−0·223	0·216
1·58	−0·055	0·041	−0·199	0·111
1·75	−0·060	0·048	−0·178	0·081
1·97	−0·051	0·041	−0·158	0·081
2·16	−0·059	0·044	−0·140	0·072
2·47	−0·049	0·035	−0·127	0·061

(*b*) blunt side edges

A.R. = 2·0, $\psi = +30°$

M	$h = 0·5$		$h = 0·6$	
	$-m_\theta$	$-m_{\dot\theta}$	$-m_\theta$	$-m_{\dot\theta}$
1·38	−0·085	0·112	−0·218	0·159
1·58	−0·052	0·076	−0·193	0·121
1·75	−0·054	0·059	−0·142	0·107
1·97	−0·047	0·049	−0·145	0·083
2·16	−0·040	0·043	−0·131	0·067
2·47	−0·037	0·052	−0·117	0·067

(*c*) sharp side edges

A.R. = 2·0, $\psi = +30°$

M	$h = 0·5$		$h = 0·6$	
	$-m_\theta$	$-m_{\dot\theta}$	$-m_\theta$	$-m_{\dot\theta}$
1·38	−0·092	0·086	−0·247	0·128
1·58	−0·049	0·071	−0·187	0·114
1·75	−0·048	0·049	−0·164	0·099
1·97	−0·046	0·047	−0·147	0·076
2·16	−0·042	0·046	−0·132	0·070
2·47	−0·038	0·048	−0·117	0·063

TABLE 3

Measured Values of the Derivatives $-m_\theta$ *and* $-m_{\dot\theta}$ *for Plain Tapered Wings of Symmetrical 5% Double-Wedge Section with Trailing Side Edges* ($\psi = -30°$)

(*a*) blunt side edges

A.R. = 2·74, $\psi = -30°$

M	$h = 0{\cdot}4$		$h = 0{\cdot}5$	
	$-m_\theta$	$-m_{\dot\theta}$	$-m_\theta$	$-m_{\dot\theta}$
1·38	0·105	0·008	−0·107	0·077
1·58	0·099	0·040	−0·063	0·061
1·75	0·059	0·045	−0·062	0·053
1·97	0·056	0·043	−0·055	0·043
2·16	0·048	0·043	−0·048	0·051
2·47	0·034	0·042	−0·050	0·047

(*b*) blunt side edges

A.R. = 2·0, $\psi = -30°$

M	$h = 0{\cdot}4$		$h = 0{\cdot}5$	
	$-m_\theta$	$-m_{\dot\theta}$	$-m_\theta$	$-m_{\dot\theta}$
1·38	0·035	0·015	−0·151	0·094
1·58	0·065	0·027	−0·092	0·062
1·75	0·044	0·037	−0·079	0·055
1·97	0·041	0·047	−0·074	0·050
2·16	0·033	0·046	−0·067	0·052
2·47	0·030	0·043	−0·055	0·049

(*c*) sharp side edges

A.R. = 2·0, $\psi = -30°$

M	$h = 0{\cdot}4$		$h = 0{\cdot}5$	
	$-m_\theta$	$-m_{\dot\theta}$	$-m_\theta$	$-m_{\dot\theta}$
1·38	0·016	0·051	−0·161	0·083
1·58	0·060	0·048	−0·086	0·062
1·75	0·025	0·045	−0·088	0·061
1·97	0·027	0·045	−0·079	0·054
2·16	0·017	0·044	−0·072	0·055
2·47	0·019	0·040	−0·064	0·044

TABLE 4

Measured Values of the Derivatives $-m_\theta$ *and* $-m_{\dot\theta}$ *for Plain Wings of Symmetrical 5% Double-Wedge Section, A.R.* $= 1{\cdot}25$ *and* $\psi = \pm 15°$

(*a*) with blunt trailing side edges

A.R. $= 1{\cdot}25$, $\psi = -15°$

M	$h = 0{\cdot}4$		$h = 0{\cdot}5$	
	$-m_\theta$	$-m_{\dot\theta}$	$-m_\theta$	$-m_{\dot\theta}$
1·38	−0·041	0·119	−0·175	0·155
1·58	−0·006	0·091	−0·124	0·107
1·75	−0·016	0·058	−0·107	0·100
1·97	−0·006	0·057	−0·102	0·076
2·16	−0·003	0·045	−0·085	0·049
2·47	−0·007	0·046	−0·075	0·060

(*b*) with blunt leading side edges

A.R. $= 1{\cdot}25$, $\psi = +15°$

M	$h = 0{\cdot}5$		$h = 0{\cdot}6$	
	$-m_\theta$	$-m_{\dot\theta}$	$-m_\theta$	$-m_{\dot\theta}$
1·38	−0·074	0·095	−0·200	0·219
1·58	−0·062	0·074	−0·176	0·140
1·75	−0·049	0·057	−0·147	0·091
1·97	−0·050	0·054	−0·139	0·110
2·16	−0·048	0·071	−0·122	0·070
2·47	−0·040	0·064	−0·106	0·064

TABLE 5

Measured Values of the Derivatives $-m_\theta$ *and* $-m_{\dot\theta}$ *for Plain Tapered Wings of Symmetrical* 5% *Double-Wedge Section, A.R.* $= 2{\cdot}74$ *and* $\psi = \pm 45°$

(*a*) with blunt trailing side edges

A.R. $= 2{\cdot}74$, $\psi = -45°$

M	$h = 0{\cdot}4$		$h = 0{\cdot}5$	
	$-m_\theta$	$-m_{\dot\theta}$	$-m_\theta$	$-m_{\dot\theta}$
1·38	0·075	−0·023	−0·105	0·067
1·58	0·097	+0·028	−0·069	0·051
1·75	0·064	+0·031	−0·066	0·042
1·97	0·045	+0·032	−0·055	0·042
2·16	0·043	+0·032	−0·051	0·041
2·47	0·042	+0·039	−0·043	0·041

(*b*) with blunt leading side edges

A.R. $= 2{\cdot}74$, $\psi = +45°$

M	$h = 0{\cdot}5$		$h = 0{\cdot}6$	
	$-m_\theta$	$-m_{\dot\theta}$	$-m_\theta$	$-m_{\dot\theta}$
1·38	−0·089	0·038	−0·282	0·194
1·58	−0·050	0·055	−0·237	0·121
1·75	−0·055	0·042	−0·171	0·095
1·97	−0·050	0·044	−0·156	0·084
2·16	−0·045	0·039	−0·138	0·072
2·47	−0·038	0·039	−0·125	0·059

TABLE 6

Measured Values of the Derivatives $-m_\theta$ and $-m_{\dot\theta}$ for Tapered Wings of Symmetrical 5% Double-Wedge Section with Blunt Streamwise Tips, and adjacent to a Cylindrical Body with a 15° Conical Nose

A.R. = 2·74

M	$h = 0{\cdot}4$		$h = 0{\cdot}5$	
	$-m_\theta$	$-m_{\dot\theta}$	$-m_\theta$	$-m_{\dot\theta}$
1·75	0·051	0·030	−0·056	0·040
1·97	0·042	0·036	−0·055	0·038
2·16	0·038	0·029	−0·049	0·041
2·44	0·023	0·040	−0·049	0·048

A.R. = 2·0

M	$h = 0{\cdot}4$		$h = 0{\cdot}5$	
	$-m_\theta$	$-m_{\dot\theta}$	$-m_\theta$	$-m_{\dot\theta}$
1·75	0·027	0·047	−0·072	0·074
1·97	0·028	0·058	−0·059	0·048
2·16	0·020	0·037	−0·057	0·044
2·47	0·018	0·054	−0·050	0·046

A.R. = 1·25

M	$h = 0{\cdot}4$		$h = 0{\cdot}5$	
	$-m_\theta$	$-m_{\dot\theta}$	$-m_\theta$	$-m_{\dot\theta}$
1·75	−0·011	0·090	−0·089	0·084
1·97	+0·003	0·059	−0·080	0·068
2·16	−0·003	0·063	−0·070	0·051
2·47	+0·008	0·049	−0·060	0·051

TABLE 7

Measured Values of the Derivatives $-m_\theta$ and $-m_{\dot\theta}$ for Tapered Wings of Symmetrical 5% Double-Wedge Section with Blunt Streamwise Tips and adjacent to a Cylindrical Body with an Ogival Nose

A.R. = 2·74

M	$h = 0{\cdot}4$		$h = 0{\cdot}5$	
	$-m_\theta$	$-m_{\dot\theta}$	$-m_\theta$	$-m_{\dot\theta}$
1·75	0·051	0·034	−0·057	0·049
1·97	0·043	0·036	−0·053	0·050
2·16	0·036	0·028	−0·049	0·041
2·44	0·024	0·039	−0·046	0·043

A.R. = 2·0

M	$h = 0{\cdot}4$		$h = 0{\cdot}5$	
	$-m_\theta$	$-m_{\dot\theta}$	$-m_\theta$	$-m_{\dot\theta}$
1·75	0·028	0·046	−0·065	0·061
1·97	0·026	0·048	−0·061	0·044
2·16	0·021	0·038	−0·056	0·043
2·47	0·020	0·053	−0·048	0·060

A.R. = 1·25

M	$h = 0{\cdot}4$		$h = 0{\cdot}5$	
	$-m_\theta$	$-m_{\dot\theta}$	$-m_\theta$	$-m_{\dot\theta}$
1·75	−0·014	0·082	−0·083	0·079
1·97	+0·004	0·059	−0·067	0·069
2·16	−0·003	0·051	−0·070	0·065
2·47	+0·006	0·051	−0·058	0·048

TABLE 8

Measured Values of the Derivatives $-m_\theta$ *and* $-m_{\dot\theta}$ *for Tapered Wings of Symmetrical* 5% *Double-Wedge Section, A.R.* $= 2{\cdot}74$ *and* $\psi = -30°$, *and adjacent to a Cylindrical Body fitted with either a* 15° *Cone or an Ogival Shape Nose*

(*a*) with blunt trailing side edges adjacent to a cylindrical body with a 15° conical nose

A.R. $= 2{\cdot}74$, $\psi = -30°$

M	$h = 0{\cdot}4$		$h = 0{\cdot}5$	
	$-m_\theta$	$-m_{\dot\theta}$	$-m_\theta$	$-m_{\dot\theta}$
1·75	0·050	0·046	−0·063	0·057
1·97	0·036	0·039	−0·059	0·046
2·16	0·037	0·037	−0·051	0·041
2·47	0·027	0·037	−0·049	0·037

(*b*) with blunt trailing side edges adjacent to a cylindrical body with an ogival nose

A.R. $= 2{\cdot}74$, $\psi = -30°$

M	$h = 0{\cdot}4$		$h = 0{\cdot}5$	
	$-m_\theta$	$-m_{\dot\theta}$	$-m_\theta$	$-m_{\dot\theta}$
1·75	0·048	0·067	−0·062	0·055
1·97	0·042	0·047	−0·060	0·054
2·16	0·048	0·036	−0·049	0·042
2·47	0·027	0·031	−0·043	0·041

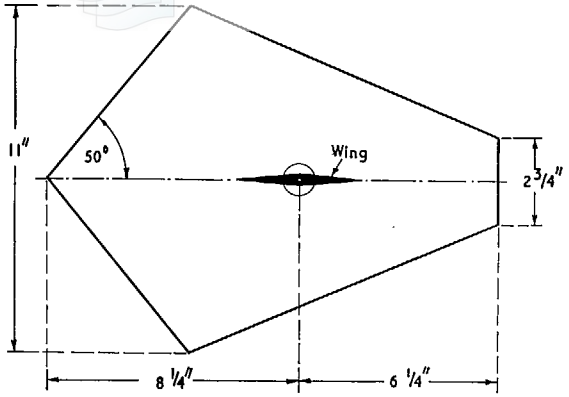

FIG. 1a. Reflection plate for Mach number $1 \cdot 35 < M < 1 \cdot 7$ used with plain wings only.

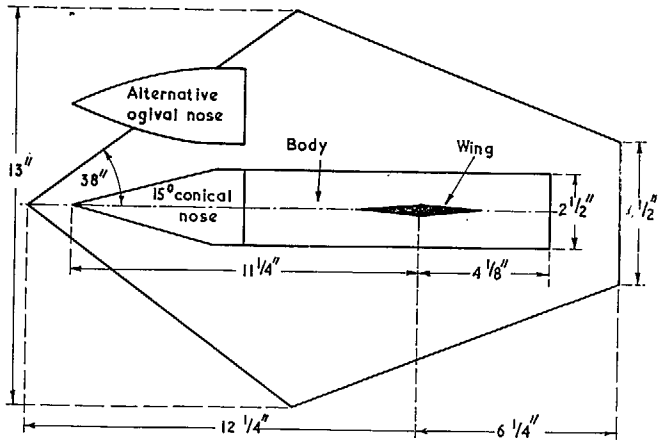

FIG. 1b. Reflection plate for Mach number $1 \cdot 75 < M < 2 \cdot 5$ used with plain wings and with wing-body combinations.

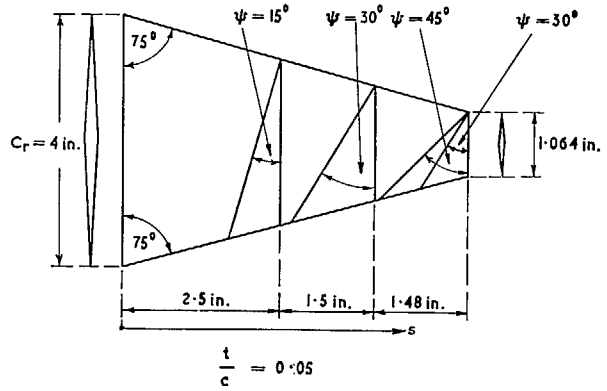

Model	ψ	S ft²	Cr ft	A. R. 2s/Cr
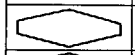	0°	0·193	0·333	2·74
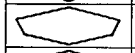	±30°	0·187	0·333	2·74
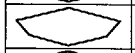	±45°	0·182	0·333	2·74
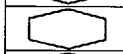	0°	0·163	0·333	2·00
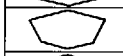	±30°	0·146	0·333	2·00
	0°	0·116	0·333	1·25
	±15°	0·101	0·333	1 25

FIG. 2. Details of plain wings tested.

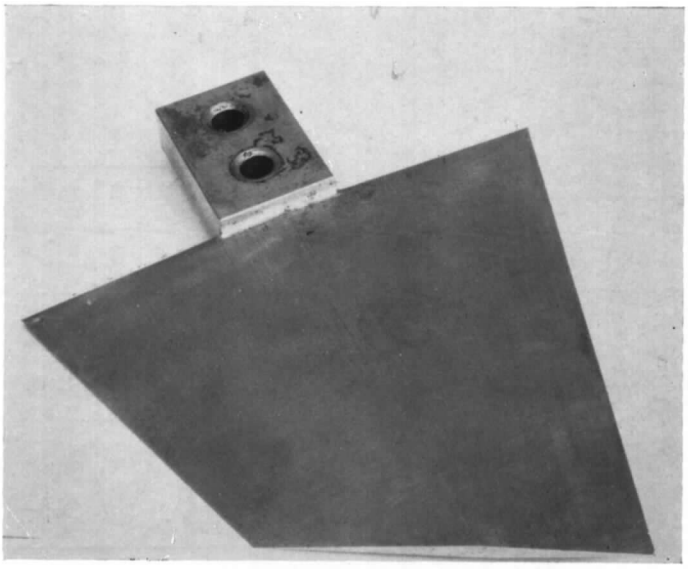

FIG. 3a. Model wing $A.R. = 2{\cdot}0$, $\psi = 30°$, with blunt side edge and attachment flange for pitching about the $h = 0{\cdot}5$ axis.

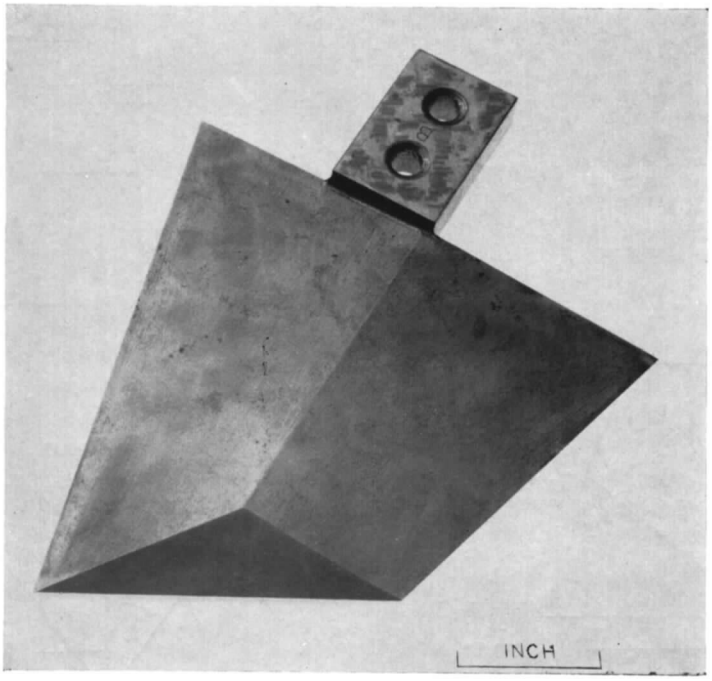

FIG. 3b. Model wing $A.R. = 2{\cdot}0$, $\psi = 30°$ with sharp side edge and attachment flange for pitching about the $h = 0{\cdot}4$ or $h = 0{\cdot}6$ axis.

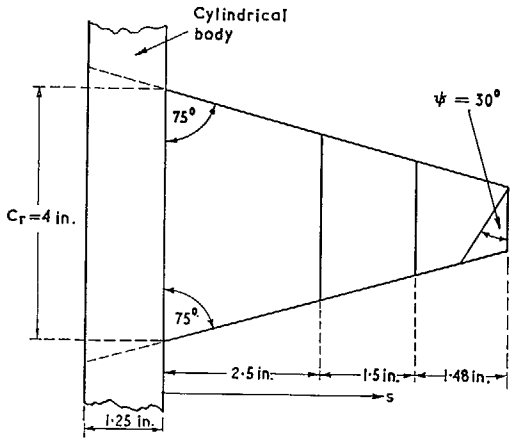

Wing–body combination	ψ	S ft²	C_r ft	A. R. $\frac{2s}{C_r}$
	0°	0·193	0·333	2·74
	0°	0·163	0·333	2·00
	0°	0·116	0·333	1·25
	30°	0·187	0·333	2·74

FIG. 4. Details of wing-body combination tested.

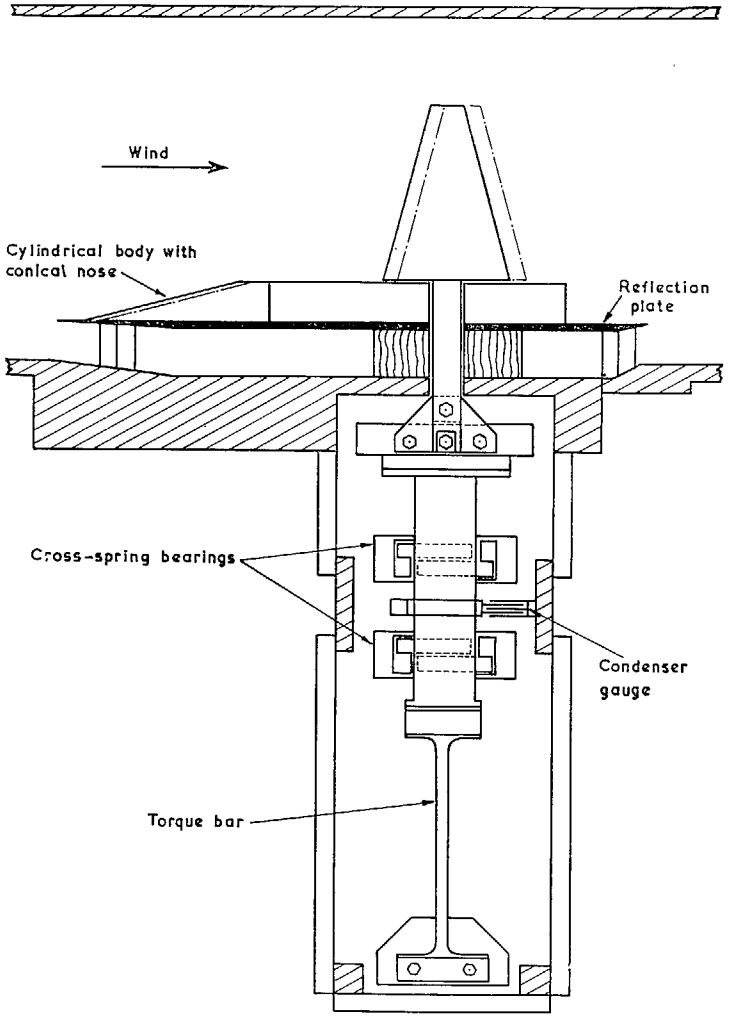

FIG. 5. General arrangement of model and spring bearing (plan view).

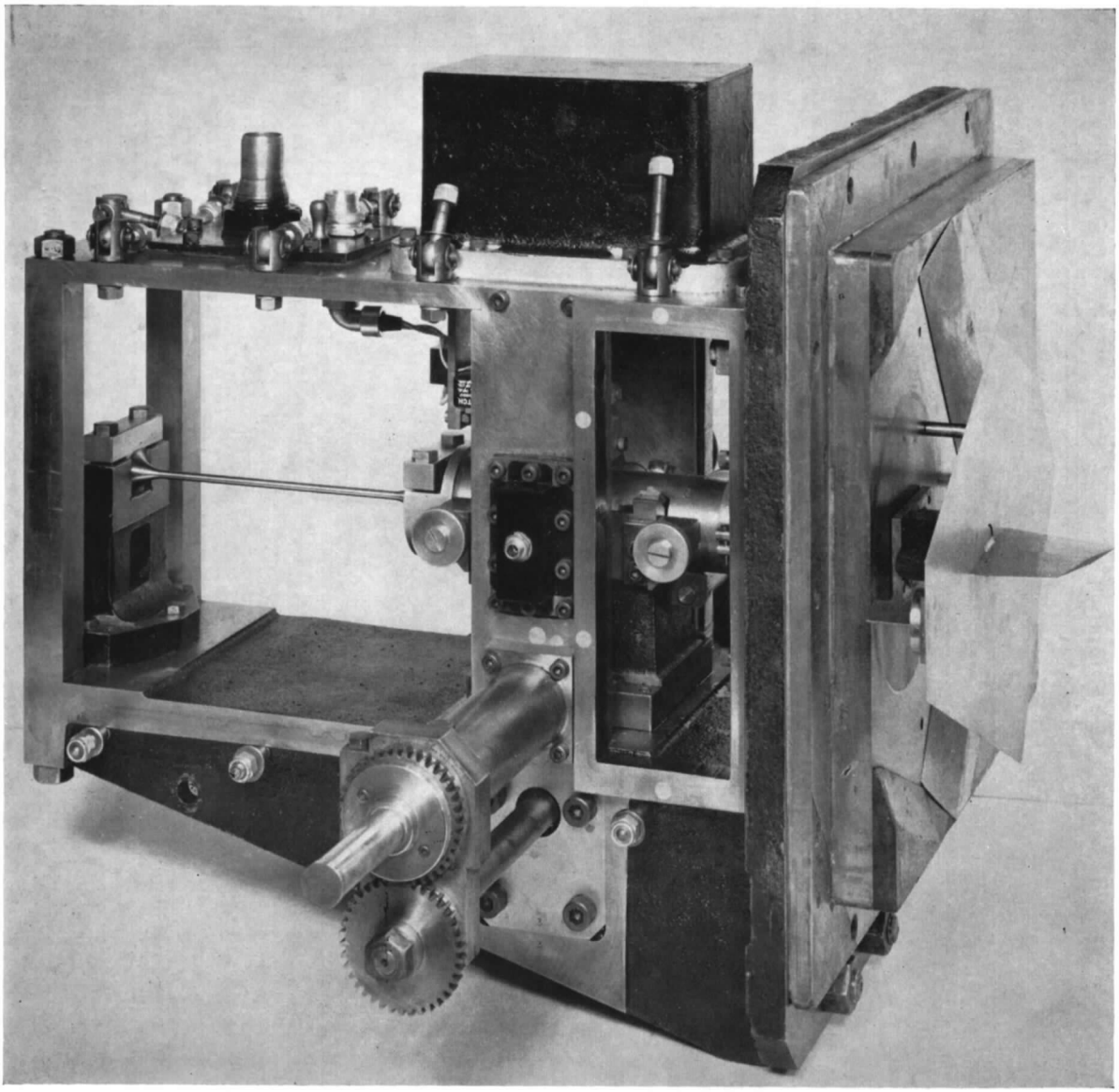

FIG. 6. Photograph of model mounting and reflection plate.

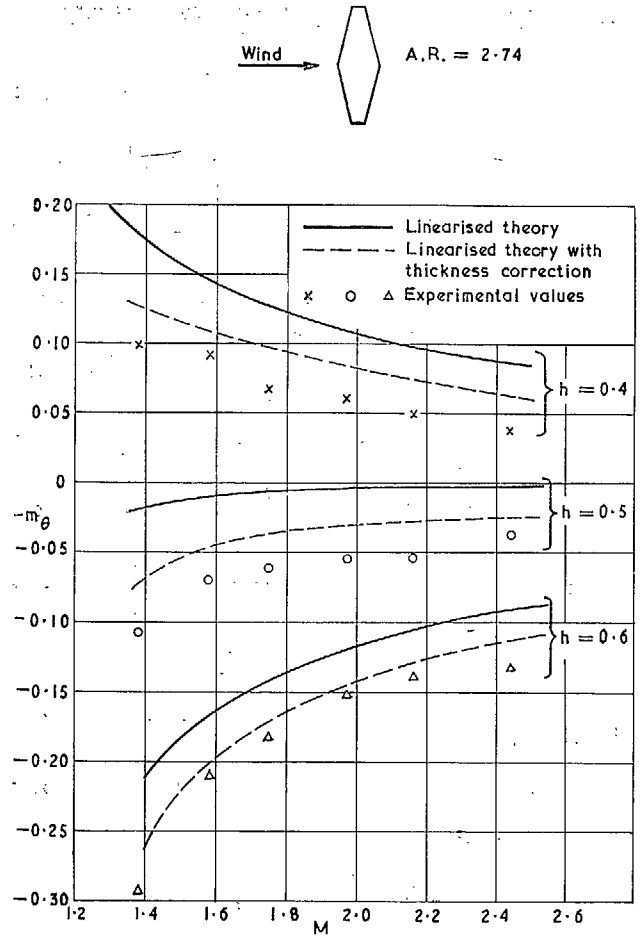

FIG. 7. Dependence of $-m_\theta$ on M for plain tapered wings of $A.R. = 2{\cdot}74$ with blunt streamwise tips.

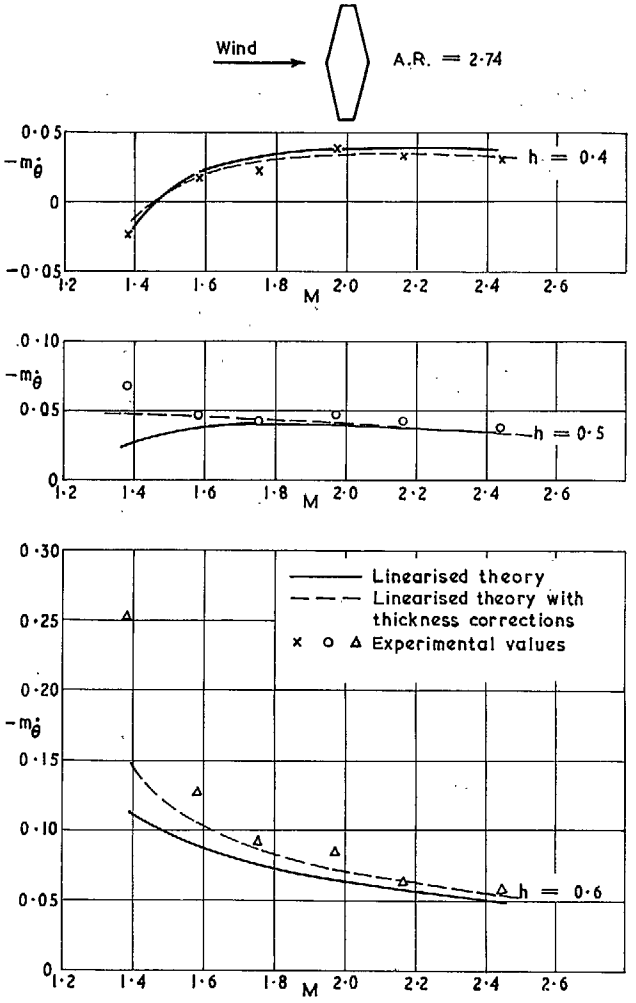

FIG. 8. Dependence of $-m_{\dot\theta}$ on M for plain tapered wings of $A.R. = 2{\cdot}74$ with blunt streamwise tips.

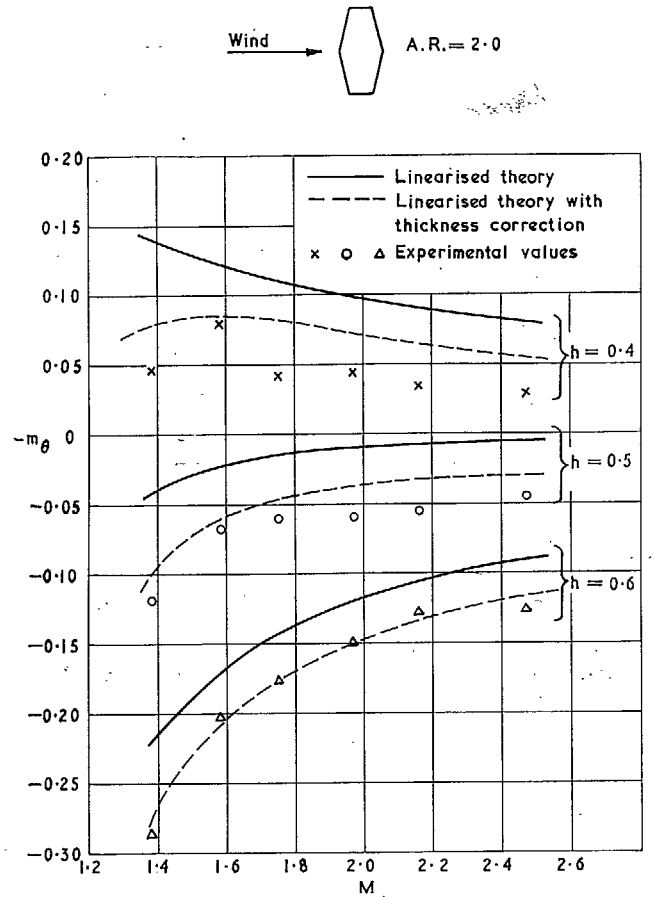

FIG. 9. Dependence of $-m_\theta$ on M for plain tapered wings of $A.R. = 2{\cdot}0$ with blunt streamwise tips.

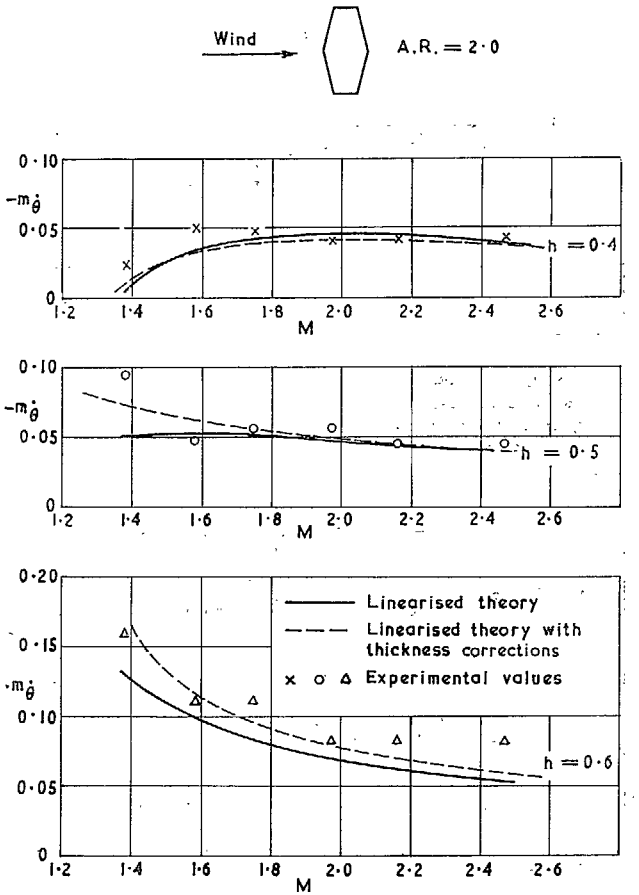

FIG. 10. Dependence of $-m_{\dot\theta}$ on M for plain tapered wings of $A.R. = 2{\cdot}0$ with blunt streamwise tips.

(85538)

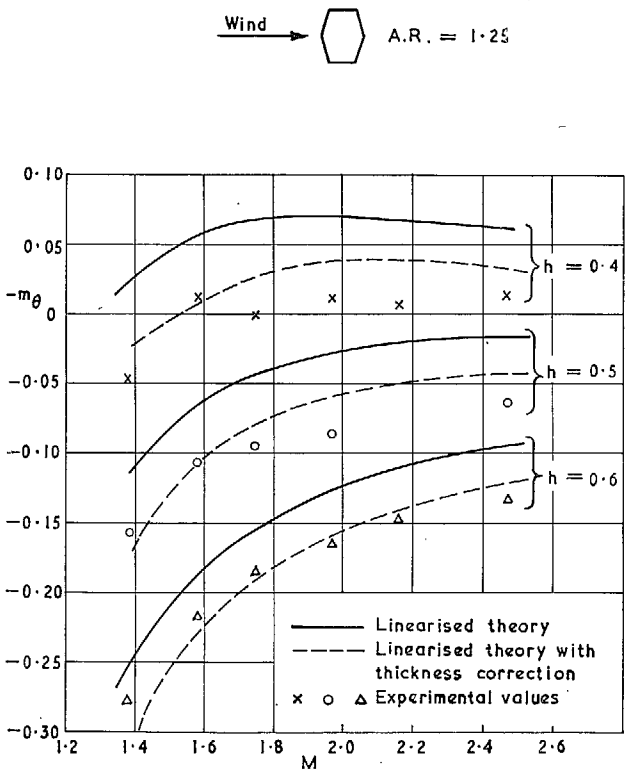

FIG. 11. Dependence of $-m_\theta$ on M for plain tapered wings of $A.R. = 1{\cdot}25$ with blunt spanwise tips.

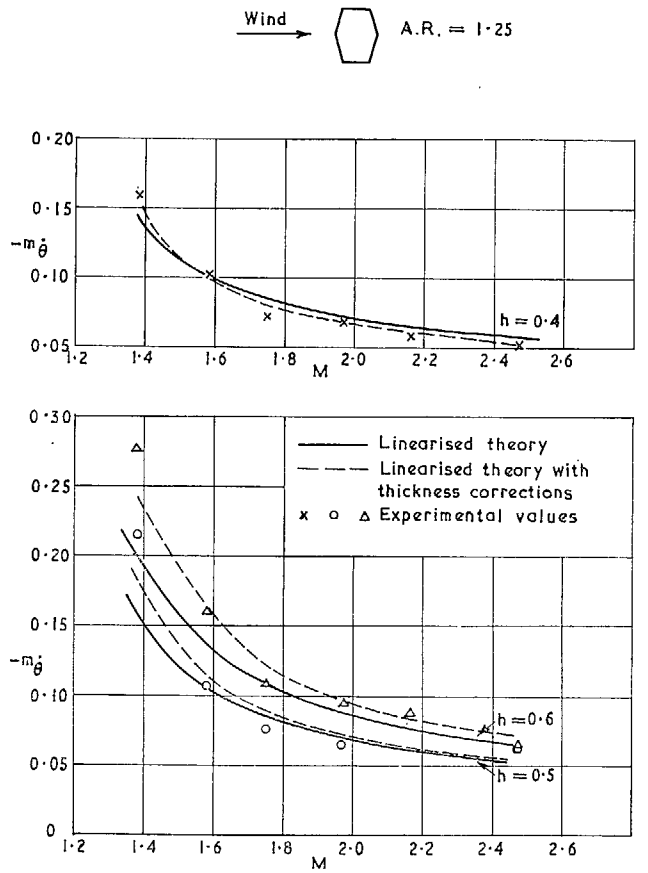

FIG. 12. Dependence of $-m_{\dot\theta}$ on M for plain tapered wings of $A.R. = 1{\cdot}25$ with blunt streamwise tips.

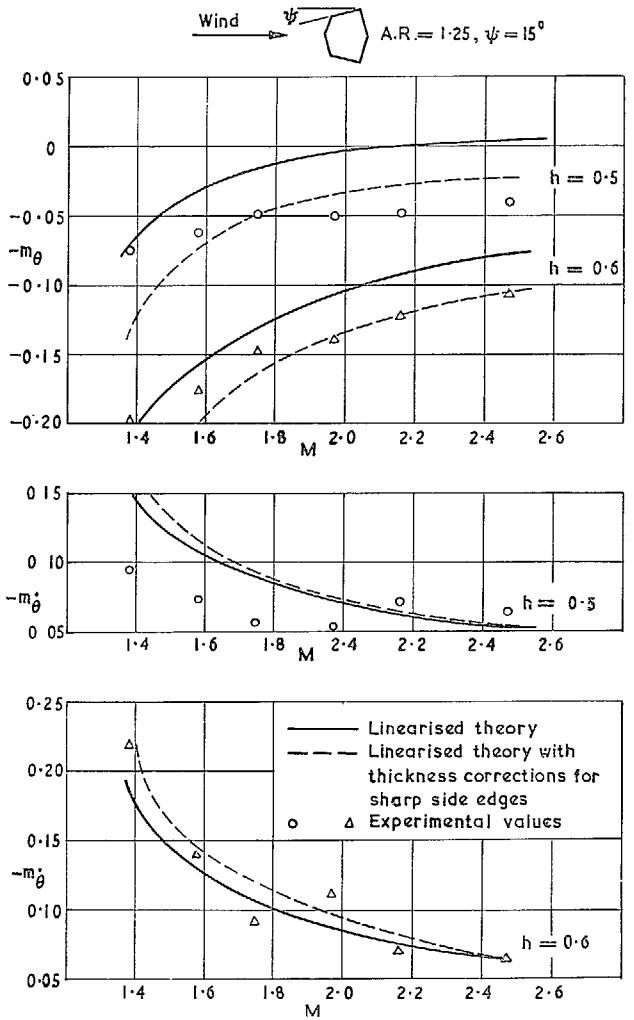

FIG. 13. Dependence of $-m_\theta$ and $-m_{\dot\theta}$ on M for plain tapered wings of $A.R. = 1{\cdot}25$ with blunt leading side edges ($\psi = +15°$).

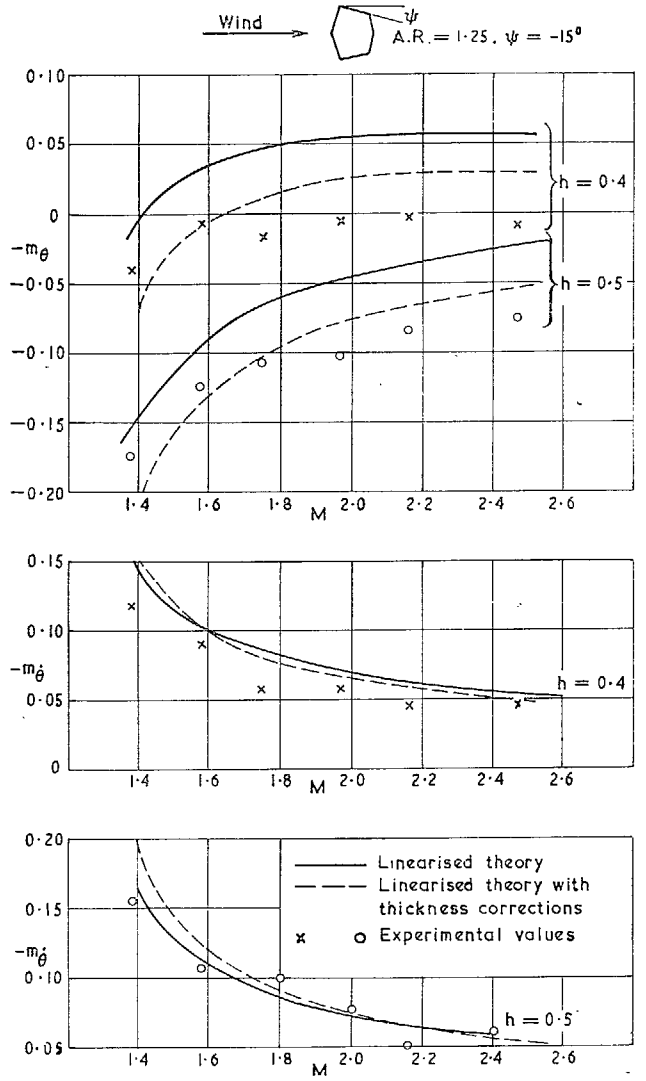

FIG. 14. Dependence of $-m_\theta$ and $-m_{\dot\theta}$ on M for plain tapered wings of $A.R. = 1{\cdot}25$ with blunt trailing side edges ($\psi = -15°$).

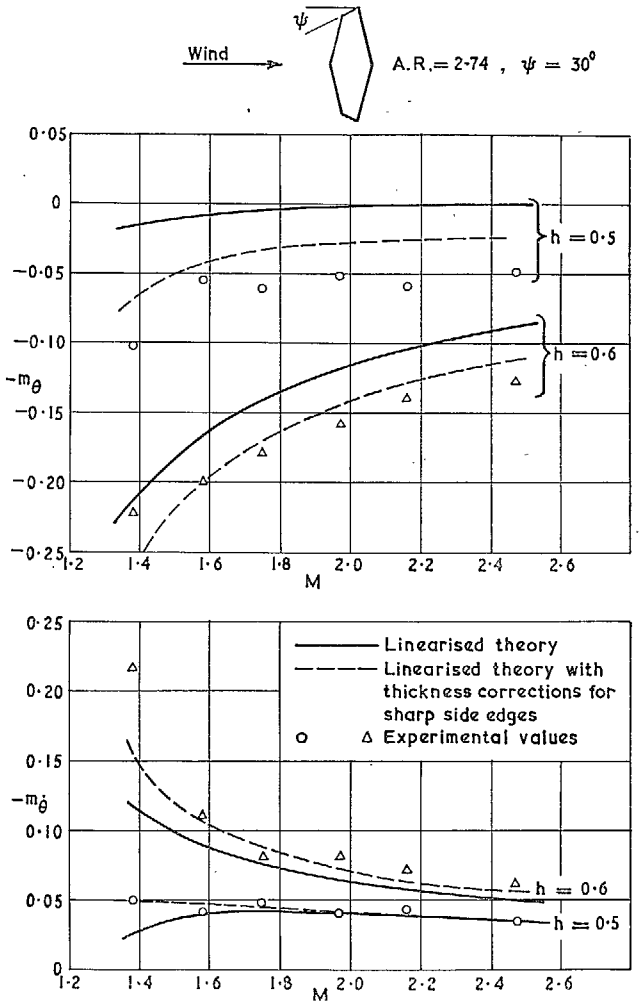

FIG. 15. Dependence of $-m_\theta$ and $-m_{\dot\theta}$ on M for plain tapered wings of $A.R. = 2{\cdot}74$ with blunt leading side edges ($\psi = 30°$).

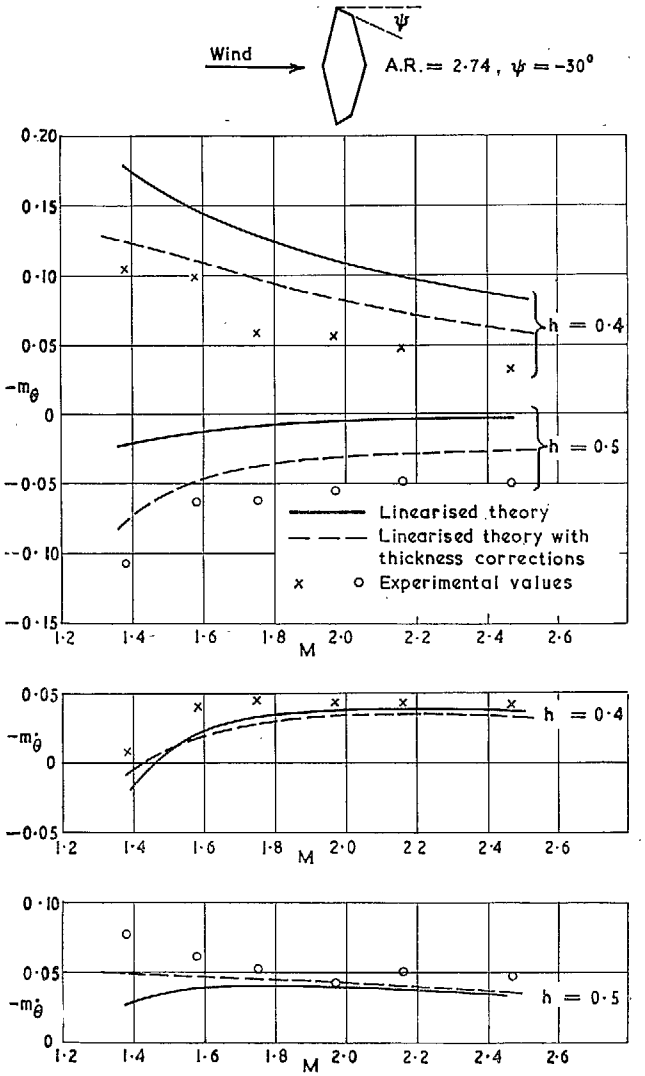

FIG. 16. Dependence of $-m_\theta$ and $-m_{\dot\theta}$ on M for plain tapered wings of $A.R. = 2{\cdot}74$ with blunt trailing side edges ($\psi = -30°$).

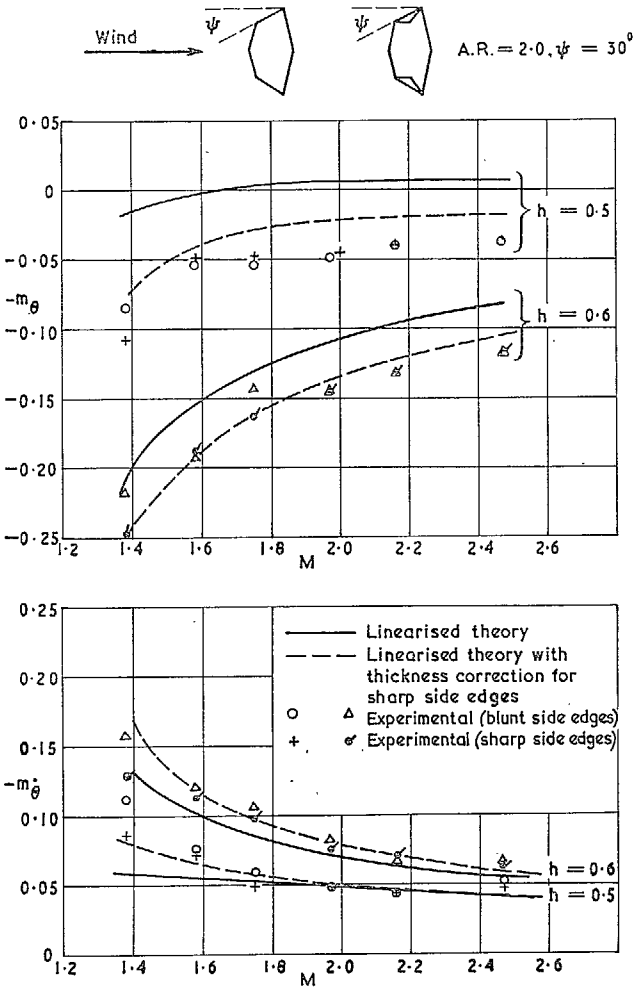

FIG. 17. Dependence of $-m_\theta$ and $-m_{\dot\theta}$ on M for plain tapered wings of $A.R. = 2{\cdot}0$ with blunt and sharp leading side edges ($\psi = 30°$).

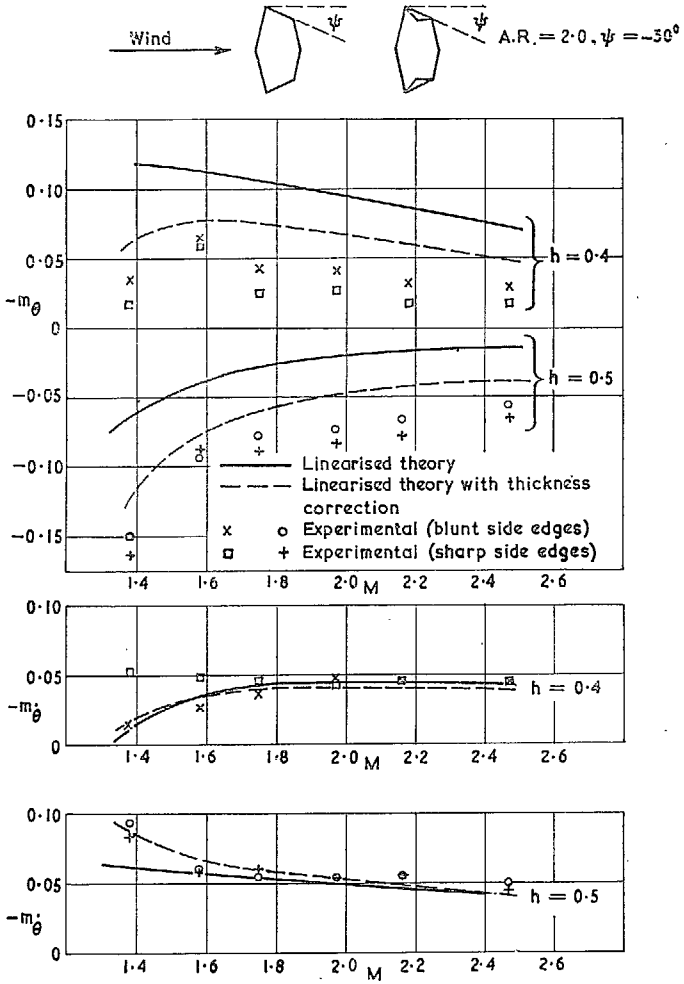

FIG. 18. Dependence of $-m_\theta$ and $-m_{\dot\theta}$ on M for plain tapered wings of $A.R. = 2{\cdot}0$ with blunt and sharp trailing side edges ($\psi = -30°$).

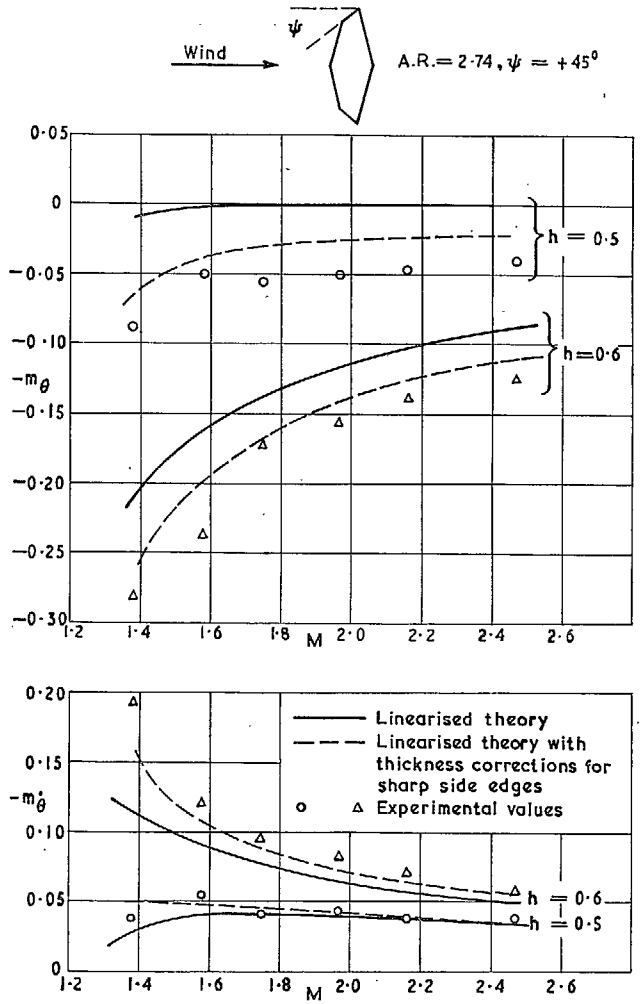

FIG. 19. Dependence of $-m_\theta$ and $-m_{\dot\theta}$ on M for plain tapered wings of $A.R. = 2{\cdot}74$ with blunt leading side edges ($\psi = +45°$).

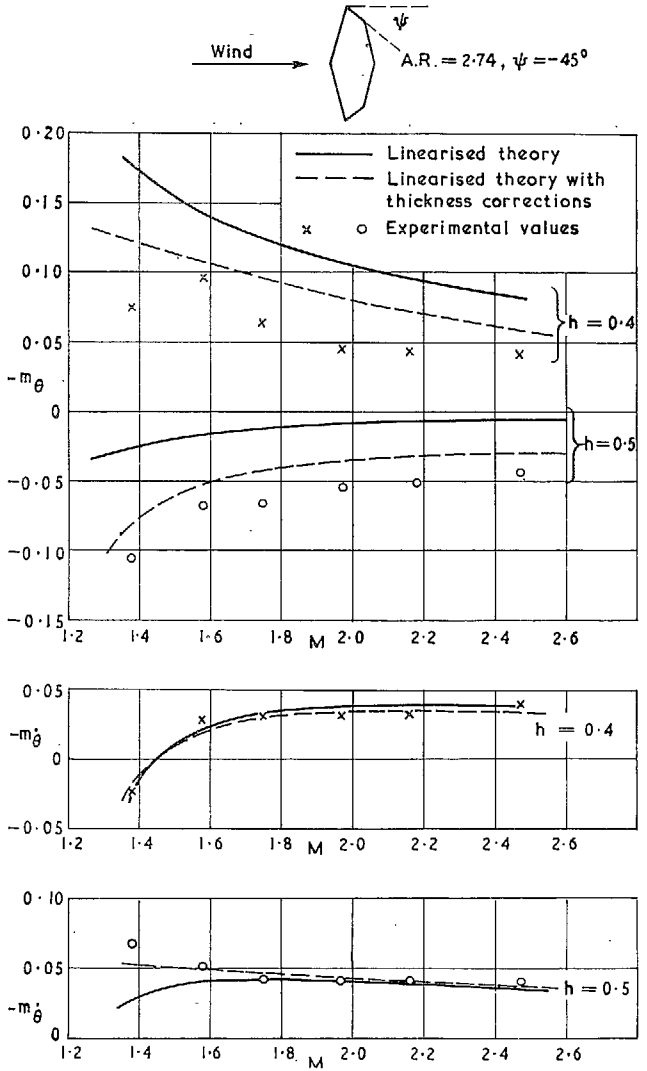

FIG. 20. Dependence of $-m_\theta$ and $-m_{\dot\theta}$ on M for plain tapered wings of $A.R. = 2{\cdot}74$ with blunt trailing side edges ($\psi = -45°$).

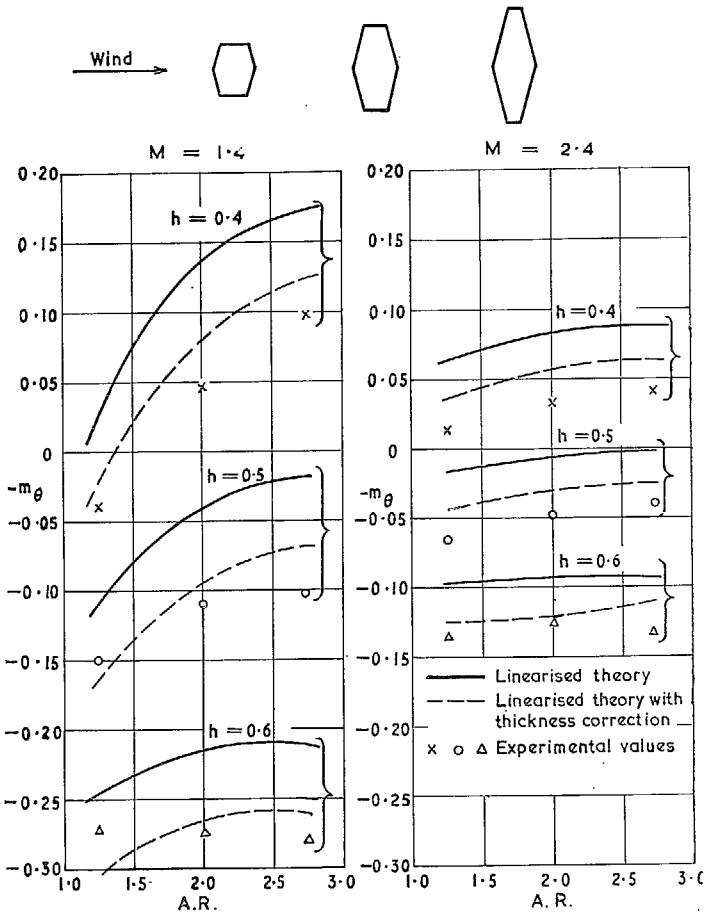

FIG. 21. Variation of $-m_\theta$ with $A.R.$ at $M = 1{\cdot}4$ and $2{\cdot}4$ (plain tapered wings with blunt streamwise tips).

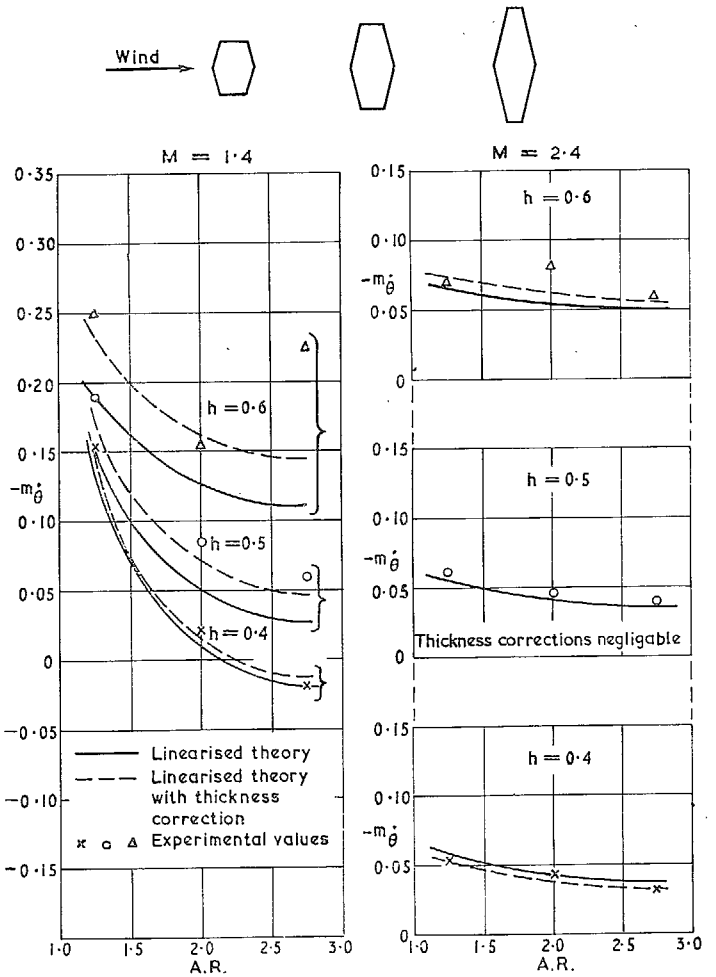

FIG. 22. Variation of $-m_{\dot\theta}$ with $A.R.$ at $M = 1{\cdot}4$ and $2{\cdot}4$ (plain tapered wings with blunt streamwise tips).

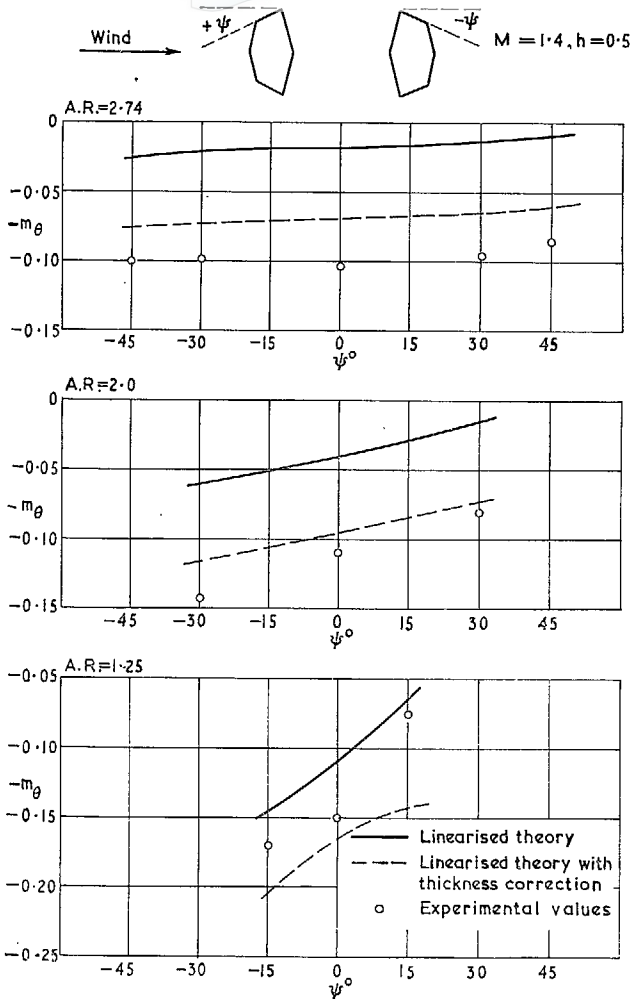

FIG. 23. Variation of $-m_\theta$ with angle of tip rake (ψ) for plain tapered wings pitching about the mid-chord axis ($h = 0{\cdot}5$) at Mach number 1·4.

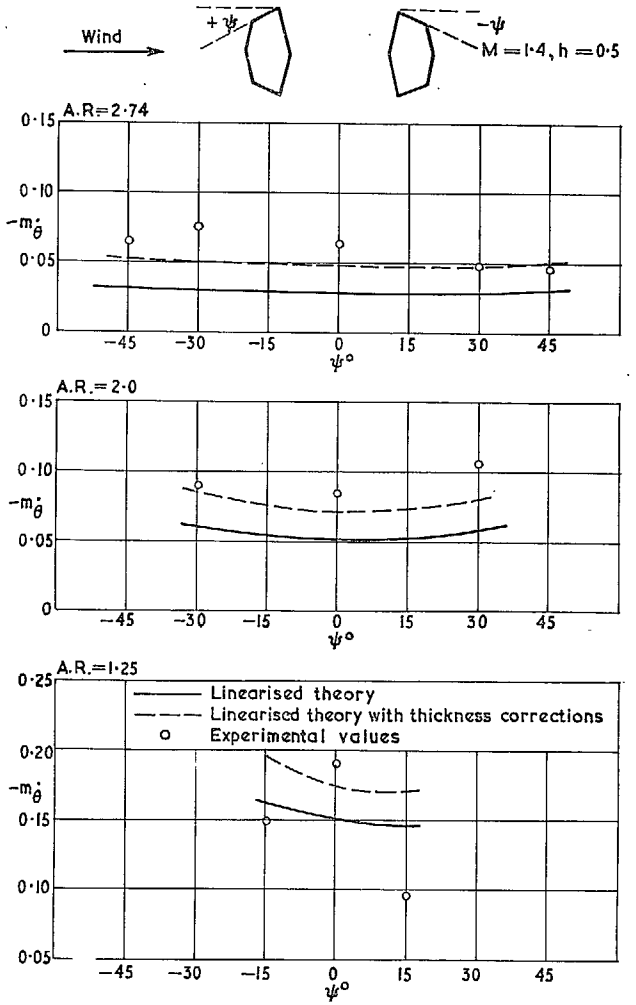

FIG. 24. Variation of $-m_{\dot\theta}$ with angle of tip rake (ψ) for plain tapered wings pitching about the mid-chord axis ($h = 0{\cdot}5$) at Mach number 1·4.

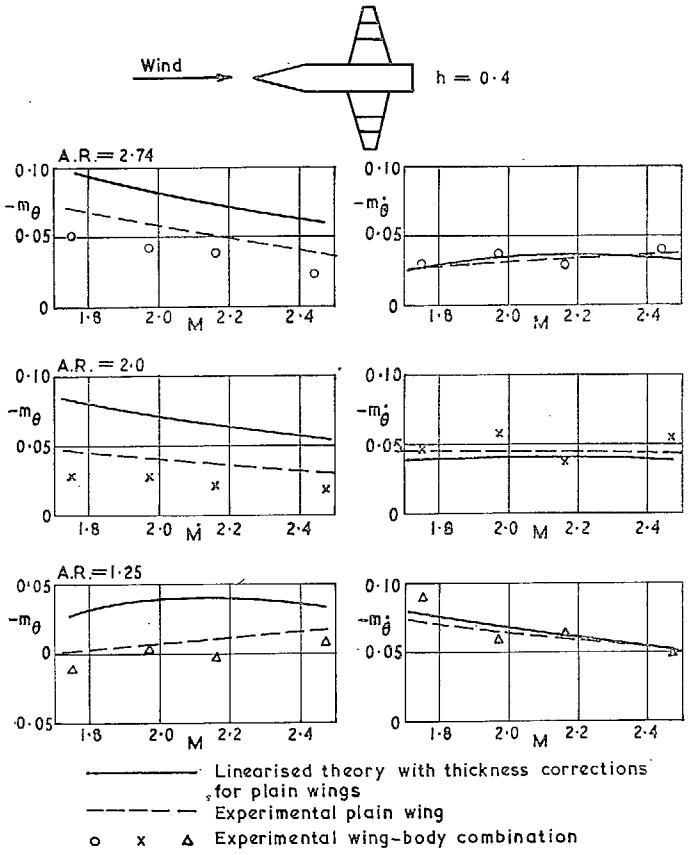

FIG. 25. Dependence of $-m_\theta$ and $-m_{\dot\theta}$ on M for tapered wings with blunt streamwise tips adjacent to a cylindrical body with a 15° conical nose ($h = 0{\cdot}4$).

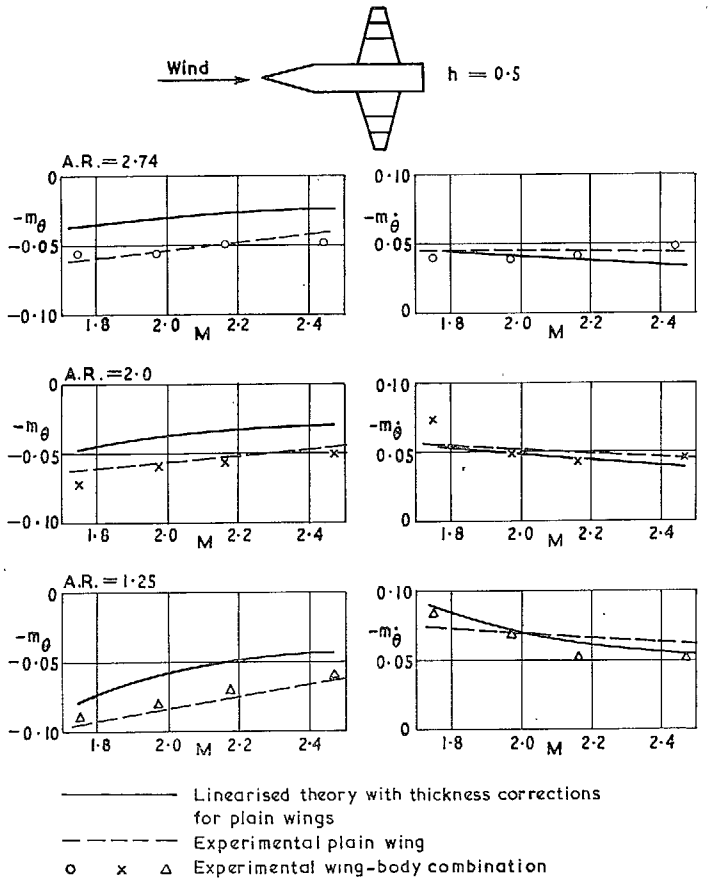

FIG. 26. Dependence of $-m_\theta$ and $-m_{\dot\theta}$ on M for tapered wings with blunt streamwise tips adjacent to a cylindrical body with a 15° conical nose ($h = 0{\cdot}5$).

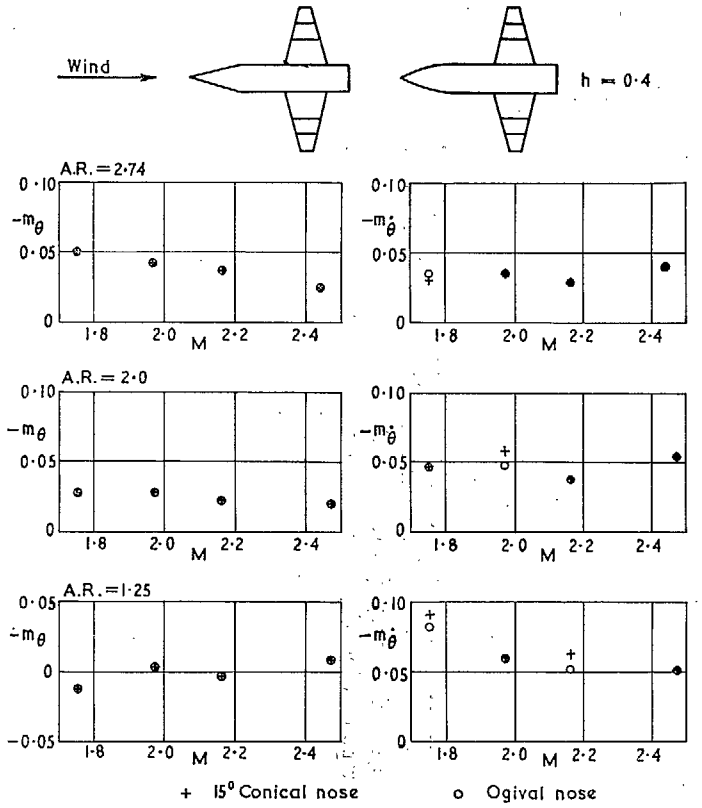

FIG. 27. Effect of nose shape on the value of $-m_\theta$ and $-m_{\dot\theta}$ for tapered wings adjacent to a cylindrical body ($h = 0{\cdot}4$).

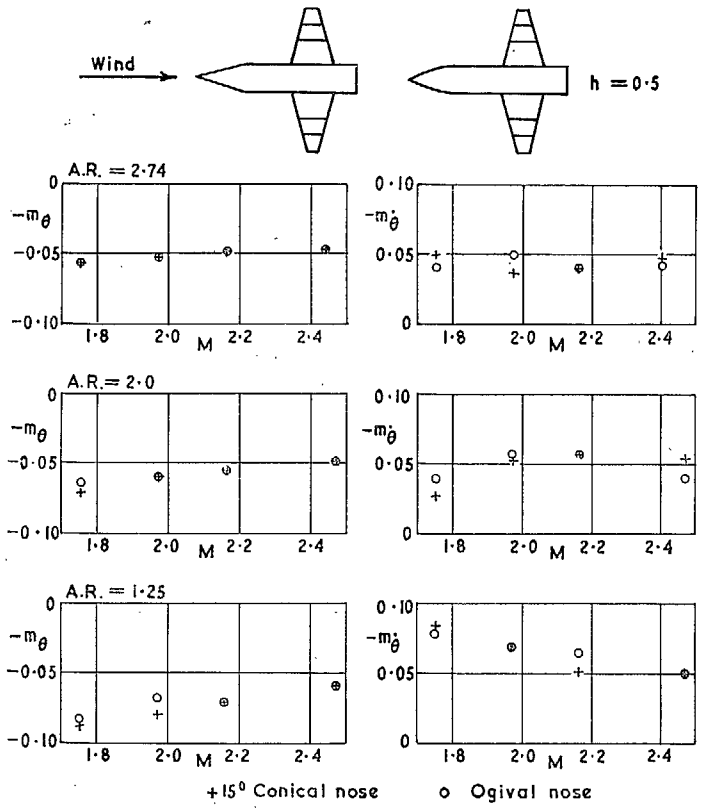

FIG. 28. Effect of nose shape on the values of $-m_\theta$ and $-m_{\dot\theta}$ for tapered wings adjacent to a cylindrical body ($h = 0{\cdot}5$).

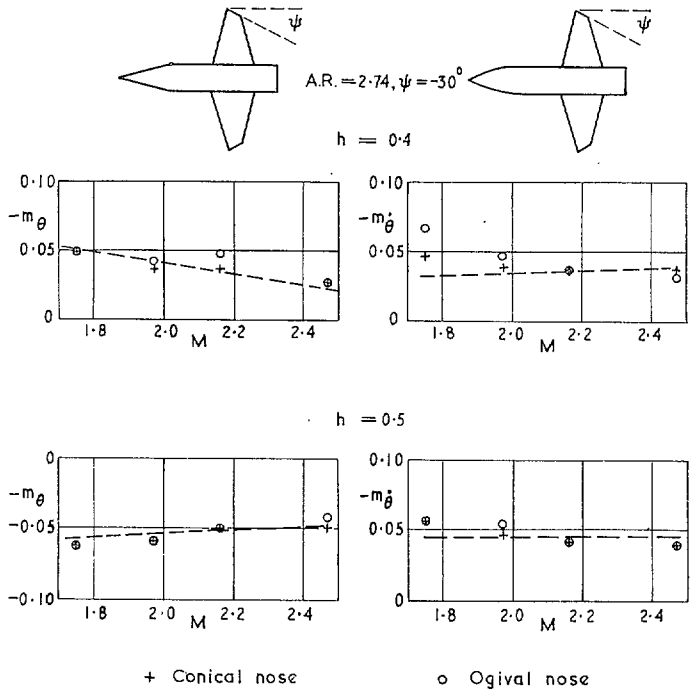

FIG. 29. Effect of nose shape on $-m_\theta$ and $-m_{\dot\theta}$ for tapered wings with blunt trailing side edges adjacent to a cylindrical body ($A.R. = 2{\cdot}74$) and comparison with a tapered wing with streamwise tips under similar conditions.

(85538) Wt. 64/1857 K5 10/62 Hw.

Publications of the Aeronautical Research Council

ANNUAL TECHNICAL REPORTS OF THE AERONAUTICAL RESEARCH COUNCIL (BOUND VOLUMES)

1942 Vol. I. Aero and Hydrodynamics, Aerofoils, Airscrews, Engines. 75*s.* (post 2*s.* 9*d.*)
Vol. II. Noise, Parachutes, Stability and Control, Structures, Vibration, Wind Tunnels. 47*s.* 6*d.* (post 2*s.* 3*d.*)

1943 Vol. I. Aerodynamics, Aerofoils, Airscrews. 80*s.* (post 2*s.* 6*d.*)
Vol. II. Engines, Flutter, Materials, Parachutes, Performance, Stability and Control, Structures. 90*s.* (post 2*s.* 9*d.*)

1944 Vol. I. Aero and Hydrodynamics, Aerofoils, Aircraft, Airscrews, Controls. 84*s.* (post 3*s.*)
Vol. II. Flutter and Vibration, Materials, Miscellaneous, Navigation, Parachutes, Performance, Plates and Panels, Stability, Structures, Test Equipment, Wind Tunnels. 84*s.* (post 3*s.*)

1945 Vol. I. Aero and Hydrodynamics, Aerofoils. 130*s.* (post 3*s.* 6*d.*)
Vol. II. Aircraft, Airscrews, Controls. 130*s.* (post 3*s.* 6*d.*)
Vol. III. Flutter and Vibration, Instruments, Miscellaneous, Parachutes, Plates and Panels, Propulsion. 130*s.* (post 3*s.* 3*d.*)
Vol. IV. Stability, Structures, Wind Tunnels, Wind Tunnel Technique. 130*s.* (post 3*s.* 3*d.*)

1946 Vol. I. Accidents, Aerodynamics, Aerofoils and Hydrofoils. 168*s.* (post 3*s.* 9*d.*)
Vol. II. Airscrews, Cabin Cooling, Chemical Hazards, Controls, Flames, Flutter, Helicopters, Instruments and Instrumentation, Interference, Jets, Miscellaneous, Parachutes. 168*s.* (post 3*s.* 3*d.*)
Vol. III. Performance, Propulsion, Seaplanes, Stability, Structures, Wind Tunnels. 168*s.* (post 3*s.* 6*d.*)

1947 Vol. I. Aerodynamics, Aerofoils, Aircraft. 168*s.* (post 3*s.* 9*d.*)
Vol. II. Airscrews and Rotors, Controls, Flutter, Materials, Miscellaneous, Parachutes, Propulsion, Seaplanes, Stability, Structures, Take-off and Landing. 168*s.* (post 3*s.* 9*d.*)

1948 Vol. I. Aerodynamics, Aerofoils, Aircraft, Airscrews, Controls, Flutter and Vibration, Helicopters, Instruments, Propulsion, Seaplane, Stability, Structures, Wind Tunnels. 130*s.* (post 3*s.* 3*d.*)
Vol. II. Aerodynamics, Aerofoils, Aircraft, Airscrews, Controls, Flutter and Vibration, Helicopters, Instruments, Propulsion, Seaplane, Stability, Structures, Wind Tunnels. 110*s.* (post 3*s.* 3*d.*)

Special Volumes

Vol. I. Aero and Hydrodynamics, Aerofoils, Controls, Flutter, Kites, Parachutes, Performance, Propulsion, Stability. 126*s.* (post 3*s.*)
Vol. II. Aero and Hydrodynamics, Aerofoils, Airscrews, Controls, Flutter, Materials, Miscellaneous, Parachutes, Propulsion, Stability, Structures. 147*s.* (post 3*s.*)
Vol. III. Aero and Hydrodynamics, Aerofoils, Airscrews, Controls, Flutter, Kites, Miscellaneous, Parachutes, Propulsion, Seaplanes, Stability, Structures, Test Equipment. 189*s.* (post 3*s.* 9*d.*)

Reviews of the Aeronautical Research Council

1939–48 3*s.* (post 6*d.*) 1949–54 5*s.* (post 5*d.*)

Index to all Reports and Memoranda published in the Annual Technical Reports

1909–1947 R. & M. 2600 (out of print)

Indexes to the Reports and Memoranda of the Aeronautical Research Council

Between Nos. 2351–2449	R. & M. No. 2450 2*s.* (post 3*d.*)
Between Nos. 2451–2549	R. & M. No. 2550 2*s.* 6*d.* (post 3*d.*)
Between Nos. 2551–2649	R. & M. No. 2650 2*s.* 6*d.* (post 3*d.*)
Between Nos. 2651–2749	R. & M. No. 2750 2*s.* 6*d.* (post 3*d.*)
Between Nos. 2751–2849	R. & M. No. 2850 2*s.* 6*d.* (post 3*d.*)
Between Nos. 2851–2949	R. & M. No. 2950 3*s.* (post 3*d.*)
Between Nos. 2951–3049	R. & M. No. 3050 3*s.* 6*d.* (post 3*d.*)
Between Nos. 3051–3149	R. & M. No. 3150 3*s.* 6*d.* (post 3*d.*)

HER MAJESTY'S STATIONERY OFFICE

from the addresses overleaf

Printed and published by
HER MAJESTY'S STATIONERY OFFICE

To be purchased from
York House, Kingsway, London W.C.2
423 Oxford Street, London W.1
13A Castle Street, Edinburgh 2
109 St. Mary Street, Cardiff
39 King Street, Manchester 2
50 Fairfax Street, Bristol 1
35 Smallbrook, Ringway, Birmingham 5
80 Chichester Street, Belfast 1
or through any bookseller

Printed in England

S.O. Code No. 23-3294